Mendeleev Commun., 2027, **37**, JUST ACCEPTED

Received 27.07.26
Revised 28.09.26

26/8161

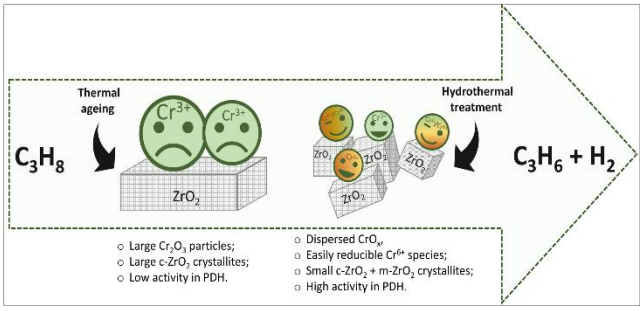
Effect of hydrothermal treatment or thermal ageing on CrO_x/ZrO_2 catalysts for nonoxidative propane dehydrogenation

Igor Yu. Kaplin,* Saveliy N. Urakhov, Ekaterina S. Lokteva, Oksana Ya. Isaikina, Konstantin I. Maslakov and Elena V. Golubina

Department of Chemistry, M. V. Lomonosov Moscow State University, 119991 Moscow, Russian Federation. Fax: +7 495 939 4575; e-mail: kaplinigormsu@gmail.com

DOI: 10.71267/mencom.8161

The influence of zirconium dioxide template synthesis parameters (hydrothermal treatment versus thermal ageing) on the catalytic properties of CrO_x/ZrO_2 in the nonoxidative dehydrogenation of propane to propylene was determined. Hydrothermal treatment ensures the formation of a mixed phase composition of ZrO_2 (monoclinic + cubic), increased dispersion of zirconium and chromium oxides, their close contact and easy reducibility, providing improved catalytic properties (19% propane conversion at 550°C with 80% selectivity to propylene) in comparison with thermally aged sample.



Keywords: propane dehydrogenation, propylene, chromium oxide, zirconia, CrO_x/ZrO_2, thermal ageing, hydrothermal treatment.

Propylene is one of the key platform chemicals for the production of polypropylene, acrylonitrile, propylene oxide and other large-scale petrochemical products. Since the propylene yield in steam cracking depends strongly on the nature of the feedstock, the increasing use of feedstock rich in light alkane has stimulated the development of the other propylene production technologies, including direct propane dehydrogenation.[1,2] Nonoxidative propane dehydrogenation is thermodynamically limited and highly endothermic reaction requiring high temperatures, which promote catalyst deactivation due to coke formation and side reactions.[1-3]

Commercially relevant propane dehydrogenation catalysts are based on Pt–Sn or chromium oxide systems.[1,3] Platinum based catalysts are highly active but expensive and prone to sintering, whereas chromium based systems are attractive due to their high activity and relatively low cost, despite environmental concerns associated with chromium compounds.[3,4] Thus, a current direction in catalyst design is the stabilization of highly dispersed chromium oxide species on rationally designed carriers at reduced chromium loading.

Zirconium oxide is a promising support and catalytic component for propane dehydrogenation because coordinatively unsaturated Zr sites formed near oxygen vacancies can participate in C–H bond activation.[5-7] The phase composition, crystallite size and reducibility of ZrO_2 strongly affect the concentration and nature of such sites.[6,7] In Cr–Zr oxide systems, the catalytic behavior is additionally controlled by the interaction between support and dispersed CrO_x species, as well as by the Cr oxidation state and redox mobility.[8-14] In particular, $CrZrO_x$ materials were shown to benefit from a synergy between zirconia derived active sites and dispersed chromium oxide species.[9-12] The particle size of the catalyst components and the degree of interaction between them can be controlled by varying the aging conditions of the gel after precipitation but prior to calcination.[15,16] Herein, we report a comparative study of three CrO_x/ZrO_2 catalysts prepared using two different post precipitation treatments of a zirconia precursor or no such treatment.

Zirconia precursors were prepared by a template assisted sol gel precipitation method using zirconyl nitrate hydrate as the zirconium source, acetylacetone as a complexing agent, Pluronic 123 as a structure directing agent, and aqueous ammonia as a precipitating agent. The next stage was different for each carrier. For the first one (further denoted as Z), the parent precursor was filtered immediately after precipitation. To produce Zr_A, the freshly precipitated gel was aged at 50°C for 13 h. For Zr_H, the gel was hydrothermally treated in a sealed autoclave at 120°C for 60 h. After drying and calcination at 600°C, 9 wt.% of chromium (chromium content calculated based on the stoichiometry of chromium (III) oxide) was introduced by impregnation with an aqueous solution of chromium (III) nitrate nonahydrate, followed by drying and final calcination in air at 600°C. The catalysts are denoted CrZr (obtained without any ageing), CrZr_A (after mild ageing) and CrZr_H (after hydrothermal treatment).

The catalysts were studied by physical-chemical methods, including atomic absorption spectroscopy (AAS), X-ray diffraction (XRD), Raman spectroscopy, X-ray photoelectron spectroscopy (XPS), and temperature programmed reduction with H_2 (H_2-TPR). The details are presented in Online Supplementary Materials (section S1).

Catalytic tests were performed in a fixed bed quartz reactor at 550°C and atmospheric pressure. The catalyst loading was 100 mg. The feed contained 40 vol.% C_3H_8 and 60 vol.% N_2, with a total flow rate of 30 mL min^{-1}. The conditions were chosen so that the reaction proceeded in a kinetic regime. The outlet gas composition was analyzed by gas chromatography. Propane conversion, propylene selectivity and the apparent propylene formation rate were calculated from chromatographic peak areas using calibration factors. Details of catalytic testing of the catalysts are described in Online Supplementary Materials (section S1).

© Mendeleev Communications.

The CrZr sample showed the lowest activity in nonoxidative propane dehydrogenation (Fig. 1). Propane conversion was only 3% after 9 min on stream, while propylene selectivity remained close to 100% during the active period. After approximately 77 min, propylene formation ceased. Thus, CrZr contains active sites that are selective to C–H activation but their concentration is very low or they are rapidly blocked under the reaction conditions.

The mildly aged CrZr_A sample was significantly more active. The initial propane conversion reached 16% after 7 min on stream with 90% selectivity to propylene. However, the propane conversion rapidly decreased; no detectable activity was observed after 52 min. The initial apparent rate of propylene formation is much higher than that for CrZr (Table 1). Therefore, ageing of the zirconia precursor increases the initial number of catalytically available sites but does not prevent fast deactivation.

The hydrothermally treated CrZr_H sample demonstrated the best catalytic behavior. The initial propane conversion was 19% after 6 min with 80% selectivity to propylene. The conversion decreased more slowly than for CrZr_A. The initial apparent rate was 0.81 mmol g_{cat}^{-1} min^{-1}, the highest value in the series.

According to atomic absorption spectroscopy (AAS), the actual chromium content was close to the nominal value of 9 wt.% Cr_2O_3 for all samples (Table 1). Therefore, the difference in catalytic behavior cannot be explained by variations in the total chromium loading and should be related primarily to the structure of the zirconia support, chromium dispersion, metal-support contact and reducibility of CrO_x species.

All XRD patterns (Figure S1) are noisy demonstrating low size of crystalline phases, and comprise reflections of the cubic ZrO_2 (Fm3m). The average crystallite size of this phase, calculated from the broadening of the c-ZrO_2 (111) reflection using the Scherrer equation, decreases in the series CrZr_A > CrZr > CrZr_H (Table 1). Also, the presence of monoclinic ZrO_2 phase is characteristic for CrZr_H and in the less extent for CrZr. This indicates that hydrothermal treatment suppresses excessive crystallite growth and results in crystal sizes comparable to those of the catalyst prepared without the aging stage. In addition, hydrothermal treatment favors the formation of finely dispersed cubic and monoclinic zirconia domains. This combination can increase the number of phase boundaries and defect sites, which are important for propane C–H bond activation over ZrO_2-containing catalysts.[17] No diffraction peaks corresponding to crystalline α-Cr_2O_3 were detected, suggesting that chromium oxide is either highly dispersed or amorphous.

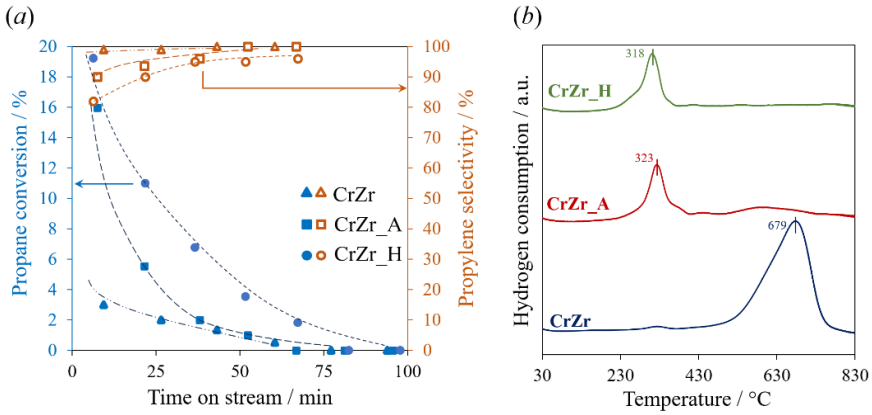


Figure 1 (*a*) Propane conversion and propylene selectivity as functions of time on stream, (*b*) H_2-TPR profiles of the catalysts.

Raman spectra (Figure S2) also showed important differences in the composition of surface species. The CrZr sample was not discussed in detail because its Raman spectrum was dominated by a high background and did not contain well-resolved bands suitable for reliable assignment.

The spectra of CrZr_A and CrZr_H differ markedly in both intensity and band resolution. CrZr_A shows only weak and broad bands at ca. 560, 650, 888 and 1020 cm^{-1}, indicating highly disordered chromium oxide species and/or a low amount of Raman-visible surface CrO_x species. The absence of crystalline α-Cr_2O_3 reflections in the XRD pattern confirms that this phase does not form large crystalline particles, but rather amorphous or highly dispersed domains. According to the literature, the band near 557 cm^{-1} can be assigned to Cr–O–Cr vibrations of Cr^{3+} species in Cr_2O_3-like domains, whereas bands in the 800 – 1000 cm^{-1} region are characteristic of oxidized Cr^{6+}-containing species, including terminal Cr=O and bridging Cr–O–Cr vibrations in polymeric chromate-like species.[11]

In comparison with CrZr_A, the hydrothermally treated CrZr_H sample exhibits more intense and better resolved Raman bands at ca. 555, 650, 700, 885 and 1025 cm^{-1}. The increasing of the intensity of these bands indicates a higher concentration of Raman-detectable, highly dispersed chromium oxide species and better structural ordering of the CrO_x–ZrO_2 interfacial region. The band at ca. 555 cm^{-1} can be related to Cr–O–Cr vibrations in highly dispersed Cr_2O_3-like domains, while the bands at 885 and 1025 cm^{-1} are assigned to oxidized chromate- or polychromate-like surface species. The additional feature near 700 cm^{-1} may be associated either with oxygen sublattice disorder in zirconia, including oxygen vacancy-related defects, or with octahedrally coordinated Cr^{3+}-containing [CrO_6] units, as discussed previously for CrZrSi catalysts.[11] Apparently, hydrothermal treatment ensures a more favorable distribution of chromium oxide species, resulting in higher activity and slower deactivation of the CrZr_H catalyst.

XPS was used to analyze the surface composition and chromium oxidation states in the catalysts. The survey spectra (Figure S3) contain signals of Zr, O, C and Cr, while high-resolution spectra were fitted into individual components corresponding to different chemical states. The content of Cr is higher on the surface of CrZr_A compared with CrZr_H (Table S1 in Online supplementary material).

A comparison of the XPS and Raman spectroscopy results reveals the key difference between the two active catalysts. CrZr_A containing more chromium on the surface provides weaker and broader Raman bands, indicating that the sample

© Mendeleev Communications.

contains chromium oxide compounds in different coordination environments; they do not form surface chromate-like compounds at the CrO_x–ZrO_2 interface. In contrast, stronger Raman features are characteristic for CrZr_H with the lower chromium content on the surface. Therefore, it includes dispersed chromate-like species and zirconia-related defect structures. These data support the conclusion that hydrothermal treatment improves the dispersion of chromium oxide and zirconia phases and the contact between them. As a result, such a catalyst exhibits higher efficiency in propane dehydrogenation.

The Cr2*p* XPS spectra (Figure S4) showed two components, which were assigned to Cr^{3+} and Cr^{6+} species, respectively. According to XPS data, the Cr^{3+} fraction on the surface decreases in the order CrZr_A > CrZr > CrZr_H. The chromium content and Cr/Zr ratio on the surface decrease in a series CrZr-_A > CrZr_H > CrZr. Both series do not coincide with the series of metal activity in the propane dehydrogenation reaction (Table S1). Thus, for the least active CrZr catalyst, the Cr^{3+} surface fraction is 83% (Table 1). Although this sample contains a noticeable amount of surface Cr^{3+} species, it exhibits the lowest initial propylene formation rate.

The surface of the most efficient in catalysis CrZr_H sample contains the minimal Cr^{3+} fraction among the studied catalysts. However, this fraction is not very small (69%), and the features of this catalyst are the smallest size of cubic ZrO_2 crystallites, significant presence of monoclinic phase and oxidized chromate- or polychromate-like surface species, as it is evident from clearly resolved Raman bands in the 885–1025 cm^{-1} region. High dispersity of chromium oxides and zirconia phases improves the contact between them and provides better catalytic efficiency of this sample compared to CrZr_A with a higher surface fraction of Cr^{3+}.

Table 1 Physicochemical characteristics of prepared samples.

Sample	Cr_2O_3[a], wt.%	D[b] / nm	$r_0(C_3H_6)$[c], mmol g_{cat}^{-1} min^{-1}	H_2 uptake[d], μmol H_2 $\cdot g_{cat}^{-1}$	Cr2*p* XPS	
					Cr^{3+}, %	Cr^{6+}, %
CrZr	9.1	5 ± 1	0.16	1620	83	17
CrZr_A	8.7	10 ± 2	0.77	315	88	12
CrZr_H	8.9	3 ± 1	0.81	360	69	31

[a] According to AAS results.
[b] The average CZ crystallite size calculated using the Scherrer equation.
[c] The initial propylene formation rate calculated using the equation for a differential fixed-bed flow reactor given in Section S1 of the Online Supplementary Materials.
[d] The total H_2 consumption was determined from H_2-TPR profiles.

H_2-TPR confirmed pronounced differences in the reducibility of chromium species depending on the type of ageing of the zirconia precursor during synthesis. The hydrogen absorption, calculated on the basis of the total chromium content in the catalysts (9 wt.% Cr_2O_3), which allows the complete reduction of Cr_2O_3 to metal, is 1776 μmol $H_2 \cdot g_{cat}^{-1}$. The CrZr sample consumed about 91% of this theoretical value (Table 1), but the main reduction maximum was located at a very high temperature (679°C). Therefore, this large hydrogen uptake should not be associated with reduction of highly dispersed Cr^{6+} species which could form the Cr^{3+} species favorable for catalysis. Instead, it indicates the predominance of aggregated or bulk chromium oxide domains, which undergo deep reduction only at high temperature. This interpretation is consistent with the general behavior of supported chromium oxide catalysts, for which isolated chromium ions, two-dimensional CrO_x overlayers and three-dimensional chromium oxide crystallites can coexist depending on the metal loading and metal–support interaction.[18]

In contrast, CrZr_A and CrZr_H exhibited low-temperature reduction maxima at 323 and 318°C, respectively, with much lower hydrogen consumptions of 315 and 360 μmol $H_2 \cdot g_{cat}^{-1}$. These values correspond to only about 18 and 20% of the hydrogen uptake which is needed for complete Cr_2O_3 reduction, indicating that only a fraction of chromium is present in a readily reducible surface form. The CrZr_A catalyst contains the highest surface chromium concentration according to XPS, but the lowest fraction of Cr^{6+} species. Therefore, its low-temperature TPR peak is attributed to reduction of a limited amount of surface CrO_x species, whereas a significant fraction of chromium is likely present as less active bulk Cr^{3+} forms.

The CrZr_H catalyst shows the lowest reduction temperature and a slightly higher hydrogen uptake than CrZr_A. Together with the highest Cr^{6+} fraction determined by XPS, this indicates the formation of highly dispersed, easily reducible chromium species stabilized on the zirconia surface. Thus, the catalytic activity follows not the total hydrogen consumption, but the availability of low-temperature reducible CrO_x species: CrZr contains a large amount of reducible chromium oxide, but mainly in bulk form, whereas CrZr_H contains the most catalytically relevant fraction of dispersed redox-active chromium species on a surface accessible for adsorption of reagents. This agrees with the conclusion of Kanervo and Krause that H_2-TPR line-shape analysis provides information on the organization and dynamic redox behavior of reducible chromium species on oxide supports.[18]

In conclusion, physical-chemical studies demonstrated, that the superior activity and slower deactivation of CrZr_H are governed not by the initial amount of surface chromium, but with the formation of highly dispersed and easily reducible CrO_x species stabilized at the CrO_x–ZrO_2 interface. Such stabilization is ensured by the close contact with two zirconia phases, both finely dispersed.

CrZr contains predominantly chromium oxide species reducible only at high temperature. CrZr_A contains more surface chromium, than CrZr_H, but its substantial part is present as Cr^{3+}-rich Cr_2O_3-like domains rather than as readily reducible interfacial CrOx species.

The authors are grateful to the Lomonosov Moscow State University for access to the XPS and TEM facilities. The work was carried out in accordance with State Assignment AAAA-A21-121011990019-4.

Online Supplementary Materials

Supplementary data associated with this article can be found in the online version at doi: 10.71267/mencom.8161

References

1 S. Chen, X. Chang, G. Sun, T. Zhang, Y. Xu, Y. Wang, C. Pei and J. Gong, *Chem. Soc. Rev.*, 2021, **50**, 3315; https://doi.org/10.1039/D0CS00814A.
2 T. Otroshchenko, G. Jiang, V. A. Kondratenko, U. Rodemerck and E. V. Kondratenko, *Chem. Soc. Rev.*, 2021, **50**, 473; https://doi.org/10.1039/D0CS01140A.
3 J. J. H. B. Sattler, J. Ruiz-Martinez, E. Santillan-Jimenez and B. M. Weckhuysen, *Chem. Rev.*, 2014, **114**, 10613; https://doi.org/10.1021/cr5002436.
4 C. K. Fonzeu Monguen, A. El Kasmi, M. F. Arshad, P. M. Kouotou, S. Daniel and Z.-Y. Tian, Ind. Eng. Chem. Res., 2022, **61**, 4546; https://doi.org/10.1021/acs.iecr.2c00813.
5 T. Otroshchenko, S. Sokolov, M. Stoyanova, V. A. Kondratenko, U. Rodemerck, D. Linke and E. V. Kondratenko, *Angew. Chem. Int. Ed.*, 2015, **54**, 15880; https://doi.org/10.1002/anie.201508731.

© Mendeleev Communications.

6 Y. Zhang, Y. Zhao, T. Otroshchenko, H. Lund, M.-M. Pohl, U. Rodemerck, D. Linke, H. Jiao, G. Jiang and E. V. Kondratenko, *Nat. Commun.*, 2018, **9**, 3794; https://doi.org/10.1038/s41467-018-06174-5.
7 Y. Zhang, Y. Zhao, T. Otroshchenko, S. Han, H. Lund, U. Rodemerck, D. Linke, H. Jiao, G. Jiang and E. V. Kondratenko, *J. Catal.*, 2019, **371**, 313; https://doi.org/10.1016/j.jcat.2019.02.012.
8 T. P. Otroshchenko, U. Rodemerck, D. Linke and E. V. Kondratenko, *J. Catal.*, 2017, **356**, 197; https://doi.org/10.1016/j.jcat.2017.10.012.
9 S. Han, Y. Zhao, T. Otroshchenko, Y. Zhang, D. Zhao, H. Lund, T. H. Vuong, J. Rabeah, U. Bentrup, V. A. Kondratenko, U. Rodemerck, D. Linke, M. Gao, H. Jiao, G. Jiang and E. V. Kondratenko, *ACS Catal.*, 2020, **10**, 1575; https://doi.org/10.1021/acscatal.9b05063.
10 S. Han, T. Otroshchenko, D. Zhao, H. Lund, N. Rockstroh, T. H. Vuong, J. Rabeah, U. Rodemerck, D. Linke, M. Gao, G. Jiang and E. V. Kondratenko, *Appl. Catal. A*, 2020, **590**, 117350; https://doi.org/10.1016/j.apcata.2019.117350.
11 E. V. Golubina, I. Yu. Kaplin, A. V. Gorodnova, E. S. Lokteva, O. Ya. Isaikina and K. I. Maslakov, *Molecules*, 2022, **27**, 6095; https://doi.org/10.3390/molecules27186095.
12 E. V. Golubina, I. Yu. Kaplin, I. K. Uzhuev, A. V. Gorodnova, O. Ya. Isaikina, K. I. Maslakov and E. S. Lokteva, *Russ. J. Phys. Chem. A*, 2023, **97**, 1860; https://doi.org/10.1134/S0036024423090054.
13 A. Zubkov, T. Bugrova, M. Salaev and G. Mamontov, *Crystals*, 2021, **11**, 1435; https://doi.org/10.3390/cryst11111435.
14 M. A. Tedeeva, A. L. Kustov, P. V. Pribytkov, N. D. Evdokimenko, B. Sarkar and L. M. Kustov, *Mendeleev Commun.*, 2020, **30**, 195; https://doi.org/10.1016/j.mencom.2020.03.022.
15 Sh. O. Omarov and N. A. Pakhomov, *Catal. Ind.*, 2021, **13**, 12; https://doi.org/10.1134/S2070050421010086.
16 E. Hong, S. W. Baek, M. Shin, Y.-W. Suh and C.-H. Shin, *J. Ind. Eng. Chem.*, 2017, **54**, 137; https://doi.org/10.1016/j.jiec.2017.05.026.
17 Y. Zhang, Y. Dai, H. Li, G. Jiang and E. V. Kondratenko, *Acc. Mater. Res.*, 2025, **6**, 589; https://doi.org/10.1021/accountsmr.4c00395.
18 J. M. Kanervo and A. O. I. Krause, *J. Catal.*, 2002, **207**, 57; https://doi.org/10.1006/jcat.2002.3531.

Received: 27th July 2026; Com. 26/8161

© Mendeleev Communications.